Received: 15 May 2025 | Accepted: 12 November 2025

DOI: 10.1111/2041-210x.70221

Methods in Ecology and Evolution

RESEARCH ARTICLE

Efficient statistical inference of turning points in animal movement data

Abdulmajeed F. Alharbi[1,2] | Paul G. Blackwell[1] | Abdulaziz Alagaili[3] | Nigel C. Bennett[4] | David Michael Scantlebury[5] | Jonathan R. Potts[1]

[1]School of Mathematical and Physical Sciences, University of Sheffield, Sheffield, UK

[2]Statistics & Operations Research Department, King Saud University, Riyadh, Saudi Arabia

[3]Department of Zoology, King Saud University, Riyadh, Saudi Arabia

[4]Department of Zoology and Entomology, Mammal Research Institute, University of Pretoria, Pretoria, South Africa

[5]School of Biological Sciences, Queen's University Belfast, Belfast, UK

Correspondence
Abdulmajeed F. Alharbi
Email: aalharbi10@ksu.edu.sa

Funding information
King Saud University, Grant/Award Number: ORF-RC-2025-1900

Handling Editor: Chris S. Sutherland

Abstract

1. Recent years have seen a proliferation of high-frequency animal movement data, often at greater than 1 Hz, allowing us to gain much greater insight into behaviour than with lower frequency data. In particular, it is becoming possible to detect the precise points at which animals are making decisions to turn, thus placing the idea that the animals move in 'steps and turns' onto rigorous grounding.
2. Despite this, current efforts to ascertain the points at which animals turn tend to rely on the user making pre-determined choices of certain model parameter values. Furthermore, whilst they may give good results, there is often no theory explaining why the inferred turning points are most likely to be correct, for example by maximising a likelihood function.
3. Here, we propose a theoretically grounded statistical technique to find turning points in high-frequency movement data that does not require any a priori choices of parameter values. By testing our algorithm on simulated data, we show that our technique is both fast (e.g. 3 s to parse 10^6 data points) and accurate. For example, when the standard deviation of the noise is less than around $\frac{\pi}{12}$ radians then our algorithm correctly identifies nearly 100% of the turning points, providing the noise is not heavily autocorrelated. Additionally, we demonstrate the effectiveness of our technique on magnetometer data from free-ranging Arabian oryx (*Oryx leucoryx*).
4. Overall, our work gives a fast, accurate and statistically grounded algorithm for turning point detection in high-frequency data. The resulting model of straight-line steps and turns provides a biologically meaningful summary of the animal's movement behaviour, which has potential to be used as an input to the wide range of step-and-turn techniques used in movement ecology, such as step selection analysis and hidden Markov models of behavioural states.

KEYWORDS
animal movement, biologging, change-point detection, functional pruning optimal partitioning, high-frequency data, movement ecology, turning points

1 | INTRODUCTION

All life history goals of animals involve movement (Nathan et al., 2008). Therefore, understanding reasons behind animals' decisions to move is of crucial importance for behavioural ecology, as well as having broad applications to fields such as disease ecology (Boulinier et al., 2016) and conservation (Katzner & Arlettaz, 2020). However, inferring decisions from locational data can be tricky. If locations are measured quite infrequently then we may not have data at the point at which a decision is made. On the other hand, high-frequency data by its nature contain a lot of information that simply reflects the animal continuing on a trajectory that it has already decided upon, and therefore may contain little behavioural information (Williams et al., 2020)—the 'big data problem', Lewis et al. (2018). It therefore helps to demarcate the places on a trajectory where the animal is likely to have made an active decision about where to move (Munden et al., 2021).

Often, animals will move naturally in straight lines, turning when there are beneficial reasons for them to do so (Gunner et al., 2024). Thus turning points (changes in movement direction) implicitly contain valuable behavioural information that can be inferred by analysing correlations between turning occurrences and other covariates that might affect movement (e.g. the animal's environmental data). Armed with such knowledge, we ought to be able to make better inference in step-and-turn-based methods of inference, such as step selection analysis (Avgar et al., 2016; Munden et al., 2021) and hidden Markov models (Grainger & Blackwell, 2025; Klappstein et al., 2023; Langrock et al., 2012).

Various efforts to find these turning points have been proposed over the years (Codling & Plank, 2011; Potts et al., 2018; Turchin et al., 1991), which all require that data are gathered at frequencies much higher than the frequency of turning. Although such data were rare in the past, recent advances in biologging devices have enabled tracking data at very high frequencies, often at several measurements per second (Bidder et al., 2015; Nathan et al., 2022; Williams et al., 2020).

To fully exploit these high-resolution data, researchers increasingly rely on motion sensors capable of capturing fine-scale animal movement dynamics. Accelerometers which detect changes in velocity, magnetometers which capture heading information based on Earth's magnetic field, and gyroscopes capture body orientation. Combined, these sensors enable dead-reckoning—a technique that estimates the animal's path by updating position continuously based on speed and direction. Although powerful, dead-reckoning is subject to cumulative error and requires periodic GPS correction (Bidder et al., 2015).

Whilst these high-frequency datasets offer great opportunity for ascertaining the places animals made turns, they typically contain a very large number of datapoints, so they are unwieldy to analyse. Indeed, early techniques, such as those of Turchin et al. (1991), Cleynen et al. (2014), and Codling and Plank (2011), are unable to perform accurate inference in a reasonable timeframe (Potts et al., 2018). This prompted Potts et al. (2018) to develop a rapid technique for turning points identification in high-frequency data.

However, this method has two major shortcomings. First, it requires two a priori parameter choices: the size of the sliding window and a threshold angle below which a proposed 'turn' is too small to be considered a turn. Second, there is no rigorous statistical underpinning to the method. For example, it would be helpful to know for sure that a turning point identification method maximises a particular likelihood (or penalised likelihood) function. This would give assurance to the user, as well as detailed insight into what the method has actually shown (what model it has fitted, what assumptions are being made about the structure of error terms etc.).

Here, we develop a model-based method for turning point analysis which runs quickly on large datastreams and does not require a priori specification of parameter values. The model assumes that observed bearings, measured using magnetometry, are a noisy representation of the underlying movement direction, which remains constant over time except at turning points where shifts in direction occur. This approach enables precise and efficient detection of turning points in high-frequency animal movement data whilst minimising the need for pre-processing and arbitrary choices.

To evaluate the performance of our algorithm, we construct simulated trajectories of straight-line segments connected by sharp turns, plus noise terms of various different magnitudes and levels of autocorrelation. These terms are designed to mimic the errors inherent in data collection and the natural movement-related noise caused by animal locomotion. This setup allows us to assess the algorithm's accuracy in identifying true turning points. Our simulation study demonstrates that our algorithm is accurate and efficient, outperforming previous methods in most cases. We then apply our method to magnetometer data from free-ranging oryx, demonstrating the algorithm's ability to identify turning points in empirical data.

2 | MATERIALS AND METHODS

2.1 | Model formulation

The aim of our algorithm is to take a high-frequency time series of measured animal headings (e.g. from a magnetometer) and demarcate the points where the animal made a decision to turn from those that reflect noise in the data-gathering process. The required dataset is thus a sequence of n observed headings, evenly spaced in time, denoted by $\{h_t\}_{t=1}^{n}$, and measured in radians. First, we will start with a simple model whereby the animal's true headings are assumed to be an angular piecewise constant function of time as follows

$$h_t = \mu_t + \epsilon_t \pmod{2\pi}, \tag{1}$$

with $\mu_t = \mu_{t-1}, t \notin \{\tau_1, \ldots, \tau_m\}$. Here, $\{\tau_1, \ldots, \tau_m\}$ is a set of m turning points, μ_t represents the animal's actual heading at time t and

remains constant between any two turning points, and ϵ_t are independent and identically distributed (i.i.d.) random variables, defined on the circle, with zero circular mean. Since we anticipate shifts in the animal's direction, estimating the parameter μ_t in Equation (1) can be viewed as a change-point detection problem, where our goal is to identify shifts in the mean of the underlying process. We estimate these shifts by identifying each time step t such that $\mu_t \neq \mu_{t-1}$. Assuming the ϵ_t are i.i.d. from a von Mises distribution with zero mean and concentration parameter κ_μ, the log-likelihood of our model is

$$\mathcal{L}_{\text{IID}}\left(\{\mu_t\}_{t=1}^n \mid \{h_t\}_{t=1}^n, \kappa_\mu\right) = \kappa_\mu \sum_{t=1}^{n} \cos(h_t - \mu_t). \tag{2}$$

One particular type of data to which we might fit our model is magnetometer data. However, magnetometer data often exhibit autocorrelated error, violating the i.i.d. assumption. To address this, one approach is to incorporate autocorrelation into a penalty factor (see Section 2.3). Alternatively, we can reformulate the expected value of h_t as being dependent on the both the actual heading and the previous observation, as follows

$$E(h_t \mid \mu_t, h_{t-1}, \rho) = \operatorname{atan2}\big((1-\rho)\sin(\mu_t) + \rho \sin(h_{t-1}), (1-\rho)\cos(\mu_t) + \rho\cos(h_{t-1})\big). \tag{3}$$

The $\operatorname{atan2}(y, x)$ function computes the bearing of (x, y) from the origin (anticlockwise from the positive x axis, typically representing due east) and $\rho \in (-1, 1)$ is a correlation parameter that measures the influence of the observed heading at time $t-1$ on the expectation of the heading at time t. Notice that, in the absence of autocorrelation in error, that is $\rho = 0$, the expectation is simply $E(h_t \mid \mu_t, h_{t-1}, 0) = \mu_t$, as in Equation (1).

The model in Equation (3) can be viewed as an angular autoregressive model of order 1, or angular AR(1). This model assumes that the animal tends to move in a particular direction between turns but exhibits fluctuations around this main direction over time. Assuming the fluctuations around the expected values of h_t are i.i.d. von Mises random variables with zero mean and constant and known concentration parameter κ_ρ, the log-likelihood of our model is

$$\mathcal{L}_{\text{AR}}\left(\{\mu_t\}_{t=2}^n \mid \{h_t\}_{t=1}^n, \rho, \kappa_\rho\right) = \kappa_\rho \sum_{t=2}^{n} \cos\left(h_t - E(h_t \mid \mu_t, h_{t-1}, \rho)\right). \tag{4}$$

To clarify notation, κ_ρ in Equation (4) is the concentration parameter conditional on ρ, and κ_μ in Equation (2) is the marginal concentration around the main headings μ. For the angular AR(1) model we condition on the first observation to avoid specifying an initial distribution; this reduces the effective sample size by one and is negligible as large n is expected, so it does not affect turn detection.

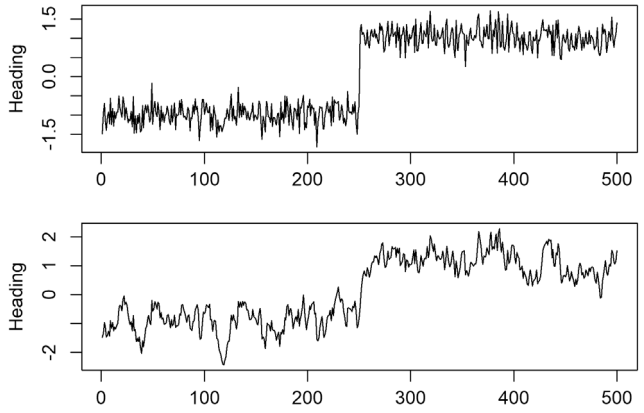

FIGURE 1 Top: Simulated heading series with single turning point assuming independent von Mises errors with $\kappa_\mu = 15$. Bottom: Simulated series with a single turning point assuming an angular autoregressive process around the mean direction with $\kappa_\rho = 15$ and $\rho = 0.80$.

Figure 1 shows example simulations of both models with a single turning point.

2.2 | Penalised maximum likelihood approach

Since adding a new parameter to a model will always increase the likelihood, simply maximising Equation (2) or Equation (4) is not sufficient; we need to penalise for the number of turning points. To address this issue, we use an additional layer of fine-tuning to control the trade-off between introducing new turning points and achieving a good fit for the estimated headings. This enables us to estimate jointly the true headings $\{\mu_t\}_{t=1}^n$, the number of turning points (m) and their locations. The resulting optimisation problem is

$$\mu_2, \ldots, \mu_n = \underset{\mu_2,\ldots,\mu_n}{\operatorname{argmax}}\left(\mathcal{L}(\{\mu_t\}_{t=2}^n \mid \{h_t\}_{t=1}^n, \rho, \kappa) + m\beta\right), \tag{5}$$

where the parameter κ refers to either κ_μ or κ_ρ, depending on the model specification, and $\beta < 0$ is a penalty term to be determined later.

To solve the optimisation problem in Equation (5), we build upon the Functional Pruning Optimal Partitioning algorithm (FPOP) introduced by Maidstone et al. (2017). The optimal penalised log-likelihood of the parameters, given the data up to time s, is denoted as follows

$$\begin{aligned} F(s) &= \max_{\mu_1,\ldots,\mu_s} \sum_{t=1}^{s}\left(Q(h_t \mid \mu_t, \ldots) + \frac{\beta_t}{\kappa}\right) \\ &= \max_{\mu_1,\ldots,\mu_s}\left(\sum_{t=1}^{s-1}\left(Q(h_t \mid \mu_t, \ldots) + \frac{\beta_t}{\kappa}\right) + Q(h_s \mid \mu_s, \ldots) + \frac{\beta_s}{\kappa}\right) \\ &= \max_{\mu_s}\left(\max_{\mu_1,\ldots,\mu_{s-1}} \sum_{t=1}^{s-1}\left(Q(h_t \mid \mu_t, \ldots) + \frac{\beta_t}{\kappa}\right) + Q(h_s \mid \mu_s, \ldots) + \frac{\beta_s}{\kappa}\right) \\ &= \max_{\mu_s}\left(F(s-1) + Q(h_t \mid \mu_t, \ldots) + \frac{\beta_s}{\kappa}\right), \end{aligned} \tag{6}$$

where $\beta_t = \beta \mathbf{1}_{\{\mu_t \neq \mu_{t-1}\}}$. Here, $\mathbf{1}_{\{\cdot\}}$ is the indicator function that is 1 if $\mu_t \neq \mu_{t-1}$ and 0 otherwise and the function $Q(h_t|\,\mu_t,\,\ldots)$ is the measurement of fit for the model (i.e. $Q(h_t|\,\mu_t) = \cos(h_t - \mu_t)$ in the i.i.d. errors case).

The function $F(s)$ can be reformulated to depend on the current heading $\mu_s = \mu$ as follows

$$F(s,\mu) = \max\left\{F(s-1,\mu), F(s-1) + \frac{\beta}{\kappa}\right\} + Q(h_s|\,\mu,\,\ldots). \tag{7}$$

In this formulation, $F(s,\mu)$ represents the maximum penalised log-likelihood for the data up to time s, conditional on the most recent actual heading being μ. In the first part of Equation (7), we assume the animal did not turn at time $s-1$ and continued moving in the same direction μ. In the second part, we assume that the last turning point occurred at time $s-1$ and that the animal has just started a new direction with bearing μ. By employing a pruned dynamic programming approach, we efficiently loop through the heading series to calculate the function $F(s,\mu)$. This process ultimately allows us to find the exact optimal sequence of headings $\{\mu_t\}_{t=1}^{n}$ as well as both the number and locations of turning points, subject to our penalised log-likelihood criterion. The dynamic programming recursion in Equation (7) can be solved for both model choices. Details are found in Appendix A in the Supporting Information.

2.3 | Estimating β, ρ and κ

The optimisation problem presented in Equation (5) requires prior knowledge of three key parameters: the noise concentration (κ), which refers to either κ_ρ or κ_μ; the autocorrelation (ρ); and the penalty term (β). In this section, we outline approaches for determining these parameters from the data.

For the penalty parameter β, we use a form that is consistent with the Bayesian Information Criterion (BIC). The full BIC expression for this model can be written as

$$\text{BIC} = (2m+3)\log(n) + n\log\left(2\pi I_0(\kappa)\right) - 2\kappa\sum_{t=1}^{n}\cos(\epsilon_t). \tag{8}$$

This can be simplified to the following form:

$$\text{BIC}/2 = m\log(n) - \kappa\sum_{t=1}^{n}\cos(\epsilon_t) + \text{constant}, \tag{9}$$

where the final term does not involve the number or location of turning points. Comparing with Equations (4) and (5), we therefore take $\beta = -\log(n)$ when using the angular AR(1).

For the IID model for autocorrelated series, an inflation factor is required, and we use $\beta = -\frac{1+\rho}{1-\rho}\log(n)$, as justified by Lavielle and Moulines (2000) and Bardwell et al. (2019). This adjustment compensates for the autocorrelation present in the data.

2.3.1 | Robust estimators based on successive difference

Estimating the noise concentration and autocorrelation is particularly challenging when the locations of the turning points are unknown. We can use the fact that for sufficiently high concentration the sum of two von Mises distributions is approximately a von Mises distribution. In particular, the circular successive differences with lag 1 are approximately von Mises distributed with zero mean and concentration parameter $\frac{(1+\rho)\kappa_\rho}{2}$. By defining the circular difference

$$d_t = (h_t - h_{t-1}) \mod 2\pi, \tag{10}$$

we expect that the location of a turning point will manifest as an outlier in the series of differences $d_2, \ldots, d_n$. This necessitates the use of a so-called 'robust' method, which minimises the influence of such outliers. Accordingly, we estimate the concentration parameter κ_d, which can be linked to the parameters of interest without requiring estimation of μ_t, as follows

$$\kappa_\rho = \frac{2\kappa_d}{1+\rho}, \quad \kappa_\mu = 2(1-\rho)\kappa_d. \tag{11}$$

we extend the approach of Fryzlewicz (2014), originally developed for data on the real line, to estimate κ_ρ and κ_μ in the context of circular data. Our adaptation accounts for the circular nature of the data by employing the angular median of the sine and cosine components of the differenced series, leading to robust estimators for both parameters:

$$\widehat{\kappa}_\rho = \frac{c}{(1+\rho)\left(1-\widetilde{R}\right)}, \tag{12}$$

$$\widehat{\kappa}_\mu = \frac{1-\rho}{1-\widetilde{R}}c, \tag{13}$$

where $c \approx 0.4592$ is a constant scale that we have estimated through a series of Monte Carlo simulations and $\widetilde{R} = \sqrt{\overline{\sin(d)}^2 + \overline{\cos(d)}^2}$ where $\overline{\sin(d)}$ and $\overline{\cos(d)}$ are the medians of $\{\sin(d_2), \cdots, \sin(d_n)\}$ and $\{\cos(d_2), \cdots, \cos(d_n)\}$ respectively.

For the estimation of ρ, in line with Chakar et al. (2017), we robustly estimate ρ as

$$\widehat{\rho} = \frac{\text{Median}_{t>2}\left(1-\cos(h_{t+2}-h_t)\right)}{\text{Median}_{t\geq 2}\left(1-\cos(h_{t+1}-h_t)\right)} - 1. \tag{14}$$

In practice, we neglect the case of negative autocorrelation due to the nature of the bearings, by setting $\rho = \max\{0, \widehat{\rho}\}$. Additionally, there is a non-zero probability that the autocorrelation estimate exceeds one, resulting in an invalid measure of autocorrelation. This risk increases when the true autocorrelation is very close to one. We will address this issue by imposing an upper limit of 1 on ρ.

2.3.2 | Non-parametric approach

A non-parametric approach offers an alternative to the estimator described in the previous section. This method involves first obtaining a preliminary estimate of the heading, and then computing κ_ρ, κ_μ, and ρ from the residuals relative to the estimated directions. One such non-parametric estimator is the moving circular median filter. Given a window of size w, the heading at time t is approximated as:

$$\widetilde{\mu}_t = \text{atan2}\left(\text{Median}\left(\sin\left(h_{(t-w/2):(t+w/2)}\right)\right), \text{Median}\left(\cos\left(h_{(t-w/2):(t+w/2)}\right)\right)\right). \tag{15}$$

The choice of window size is critical and depends on the expected minimum segment length or on the biological question at hand; a user might not need to focus on turns that occur seconds apart and may prefer to examine changes over a longer time period. A small value of w affects the estimation of ρ by removing some information about the autocorrelation and will lead to inaccurate estimation of the main direction. Given the series $\widetilde{\mu}_t$ define the centralised bearing z_t.

$$z_t = h_t - \widetilde{\mu}_t \pmod{2\pi}. \tag{16}$$

Then κ_μ and ρ can be easily be estimated from z_t where $\widehat{\kappa}_\mu$ is the maximum likelihood estimate for von Mises distribution and $\widehat{\rho}_z$ is calculated as follows

$$\widehat{\rho}_z = \frac{\sum_{t=2}^{n} \sin(z_t)\sin(z_{t-1})}{\sqrt{\sum_{t=2}^{n}\left[\sin^2(z_t)\right]\sum_{t=1}^{n-1}\left[\sin^2(z_t)\right]}} \tag{17}$$

where this measure of association between two circular variables was considered by Jammalamadaka and Sarma (1988). Given $\widehat{\rho}_z$ we estimate κ_ρ from the whitened series $\bar{z}_t$

$$\bar{z}_t = z_t - \text{atan2}\left(\rho\sin(z_{t-1}), 1-\rho\left(1-\cos(z_{t-1})\right)\right) \pmod{2\pi}. \tag{18}$$

2.4 | Simulation study

To evaluate the effectiveness of our methods, we implemented a simulation study divided into three parts. We generated three sets of simulated trajectories, each containing 50,000 data points; this sample size was chosen to be large enough to mimic real data whilst also being manageable enough to allow for thousands of replications. The scenarios varied by the number of turning points:

- *Scenario* (*A*): 158 turning points, with segment lengths ranging from 17 to 1602 time steps.
- *Scenario* (*B*): 38 turning points, with segment lengths between 167 and 4542 time steps.
- *Scenario* (*C*): A straight trajectory with no turns.

Scenarios (A) and (B) both used a minimum turning angle of $\frac{\pi}{6}$ radians. The scenarios are visualised in Figure 2. First, we assessed how our proposed methods in Section 2.3 performed in estimating ρ, κ_ρ and κ_μ. Then, we assessed the models' ability to identify turns. This evaluation was performed by introducing different error structures to the real path.

Finally, we considered different misspecification scenarios and evaluated detection robustness.

For the first task, we ran simulations for the angular AR(1) model for various values of ρ and κ_ρ. We started by setting $\rho \in \{0.3, 0.08, ..., 0.98\}$ and $\kappa_\rho \in \{5,15,45,100,200,400\}$. Each simulation was repeated 100 times, estimating ρ using Equation (14). Then, focusing on κ_ρ and κ_μ, we set $\kappa_\rho \in \{5, 10, \ldots, 400\}$ and $\rho \in \{0,0.25,0.50,0.75,0.85,0.95\}$. Again, each combination is repeated 100 times, estimating κ_ρ and κ_μ using Equation (12). We compared each estimate to the estimate obtained using the maximum likelihood estimate of κ_d.

To assess the accuracy of our method in estimating turning points, we define a turning point as detected if it is inferred to be within a certain distance of its true location. Since the choice of an acceptance threshold is somewhat arbitrary, we evaluated thresholds of 5, 10, and 20 time points, providing a clear and measurable standard for judging the model's performance. Thus, if an estimated turning point is within a certain time window from an actual turning point, it is classified as a true positive (TP); otherwise, it is a false positive (FP). Similarly, if an actual turning point does not lie within a certain distance from an estimated turning point, it is classified as a false negative (FN). If a point is not classified as a turning point, and is not within a certain number of time steps from an actual turning point, it is a true negative (TN). We replicate the simulations 10 times for each scenario. This procedure enables us to calculate the following quantities:

$$\text{Recall} = \frac{\text{TP}}{\text{TP}+\text{FN}}, \tag{19}$$

$$\text{Precision} = \frac{\text{TP}}{\text{TP}+\text{FP}}, \tag{20}$$

$$\text{F1-score} = 2\cdot\frac{\text{Recall}\times\text{Precision}}{\text{Recall}+\text{Precision}}. \tag{21}$$

To assess our detection methods, we compare the results of the detections made by the two proposed models with the application of a previous turning point algorithm introduced by Potts et al. (2018). This algorithm uses a sliding window approach, requiring specification of a window size, which we set to be $w = 40\tau$. This algorithm also post-processes the data to remove turns that are below a threshold angle θ, which we set as $\theta = \frac{\pi}{6}$ radians.

In addition to testing our inference procedure on data generated by the underlying model, we also evaluated its robustness to model misspecification in the underlying process, the error distribution, and nonconstant concentration parameters (see Appendix B in the Supporting Information).

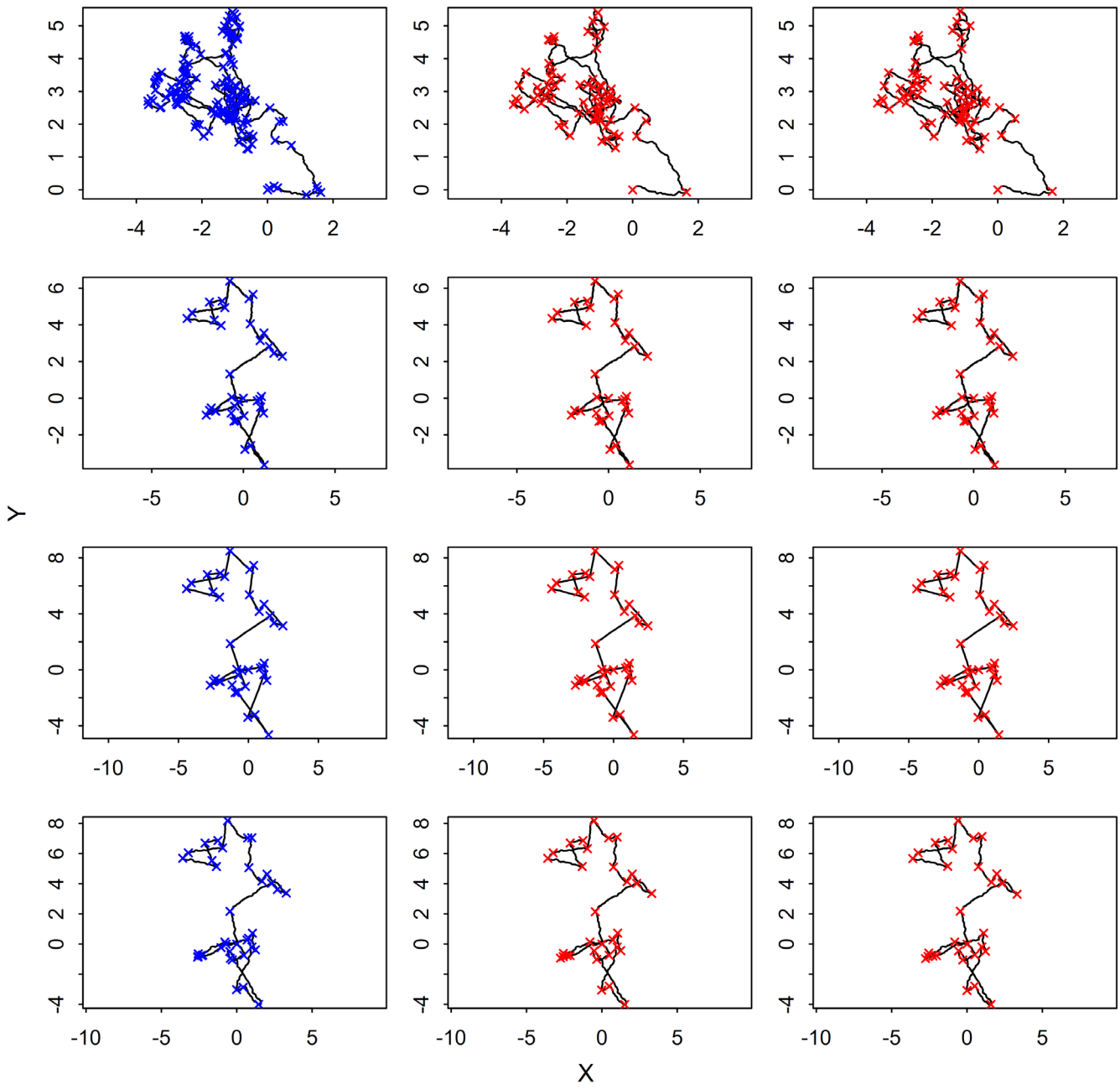

FIGURE 2 Simulated paths of headings under different scenarios. The first row shows the simulated path for scenario (A), with $\kappa_\rho = 200$ and $\rho = 0.98$. The second, third, and fourth rows correspond to scenario (B), with $\kappa_\rho = 5$, 40 and 200, and $\rho = 0.75$, 0.75 and 0.98, respectively. Blue crosses in the first column indicate the ground-truth locations of turning points, whilst red crosses in the second column show the inferred turning points using the angular AR(1) model. The third column displays the turning points inferred using the IID model.

2.5 | Case study on Arabian oryx movement

To demonstrate the effectiveness of our algorithm on empirical data, we used six trajectories from 40 Hz magnetometer data of Arabian oryx (*Oryx leucoryx*), previously used and published in Potts et al. (2018). These oryx live in Imam Saud Bin Abdulaziz Royal Reserve (formerly known as Mahazat as-Sayd), a protected desert steppe area in west-central Saudi Arabia (28°15′ N, 41°40′ E). Details of the study site and data-gathering techniques can be found in Potts et al. (2018). Ethical approval was obtained from the University of the Witwatersrand Animal Ethics Committee (2014/53/D). Permission to work in the field was granted by the President of the Saudi Wildlife Authority.

For observed trajectories, analysing the precision and recall is infeasible because we lack information on the 'true' turning points. Instead, we use the method of Potts et al. (2018), whereby

the quality of a proposed set of turning points is evaluated by creating a model path consisting of straight-line segments connecting each pair of consecutive inferred turning points, and comparing this with a path constructed directly from the data. The method computes a dimensionless quantity $\overline{\sigma} = \frac{\sigma}{l}$ where σ is a measure of the distance between the two paths and l is the average step length. Then, $\overline{\sigma}$ is a measure of the model path's goodness of fit, with lower $\overline{\sigma}$ indicating a better fit (see Potts et al. (2018) for details).

We first conducted a preliminary analysis to understand the characteristics of the noise in the data. To achieve this, we obtained a rough approximation of the signal using a moving median filter (discussed in Section 2.3). For our analysis, we set the window width to $w = 400$, equivalent to using 5 s before and after the current time step to estimate the actual heading. With the moving median estimator in place, we then constructed the residuals, which will be used to analyse the structure of the autocorrelation and estimate the noise variance.

3 | RESULTS

3.1 | Simulation study

Figure 3 compares the performance of our estimation of the autocorrelation parameter, ρ, under varying turning rates. For each value of κ_ρ (i.e. each row in Figure 3), the estimator performs similarly across the three different cases (i.e. the three columns). However, there is a notable bias as ρ increases in situations where κ_ρ is low, with the estimates tending to overestimate the true ρ for values of $\rho \gtrsim 0.5$. In other words, when the noise is large, this can exaggerate some of the autocorrelation. If the noise is reduced, that is κ_ρ is increased, this bias attenuates. This bias gradually diminishes and the estimates recover accuracy as ρ approaches higher value $\rho \gtrsim 0.9$.

Figure 4 presents simulation results comparing the robust estimator of the conditional concentration parameter, κ_ρ given in Equation (12), with the maximum likelihood estimator. In general,

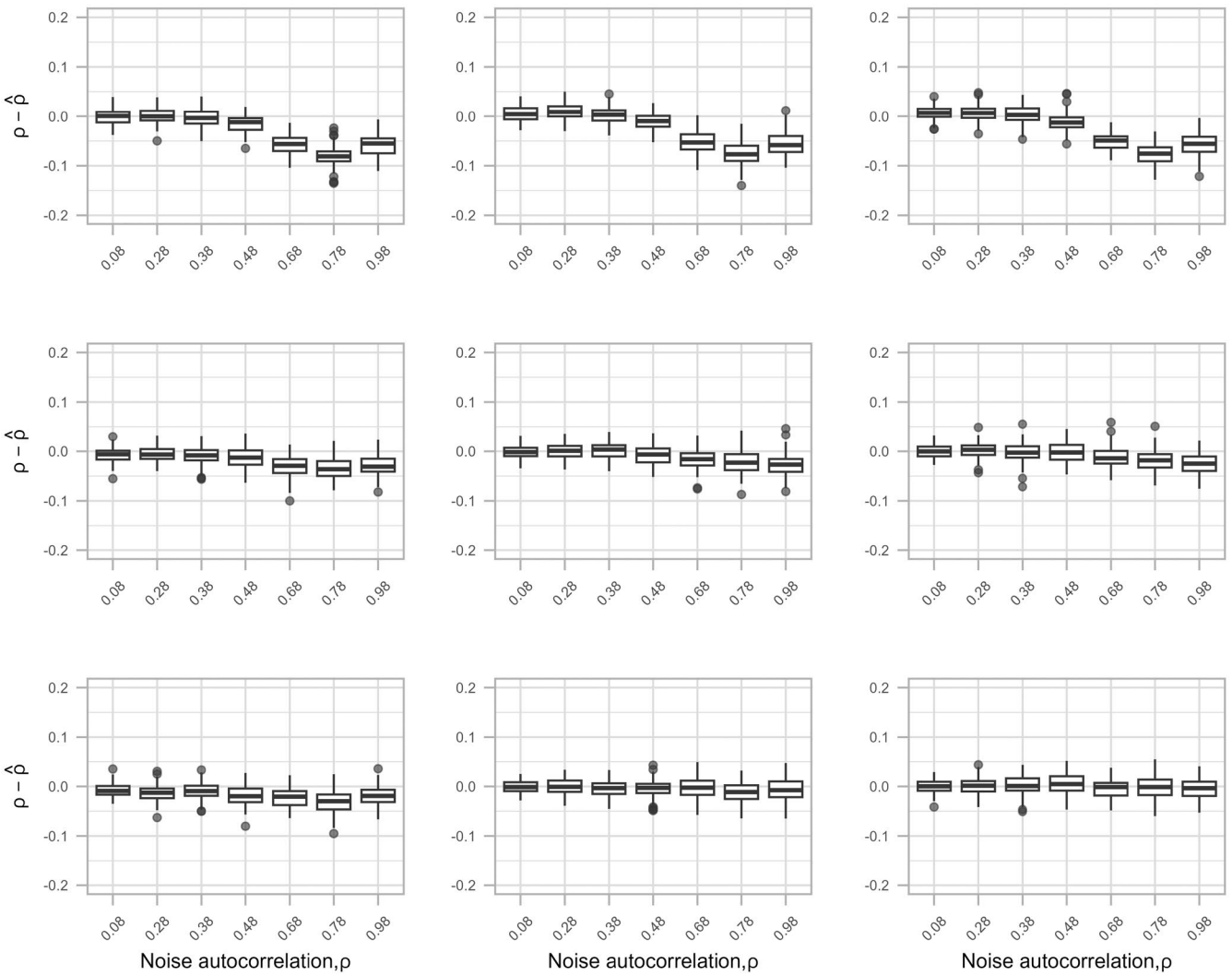

FIGURE 3 Error in estimation of ρ under the different scenarios from Section 2.4. Columns represent scenarios A, B, and C from left to right. Rows represent different κ_ρ values, with $\kappa_\rho = 5, 15$ and 45 from top to bottom.

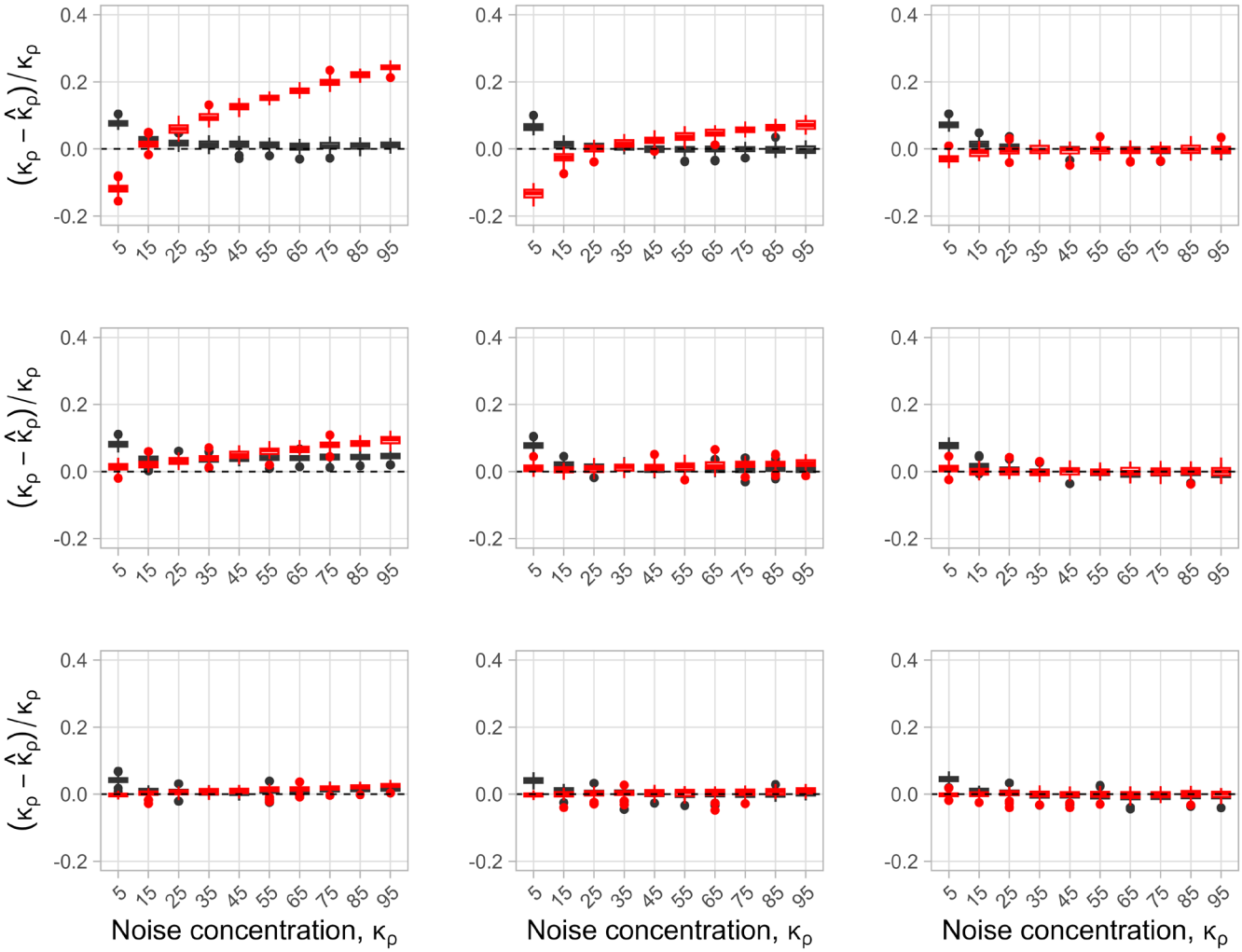

FIGURE 4 Relative error in estimation of κ_ρ under different scenarios. The columns represent A, B and C from left to right (see Section 2.4). Rows represent different ρ values, with $\rho = 0$, $\rho = 0.75$ and $\rho = 0.95$ from top to bottom. The black boxplots represent the errors made by our robust estimator, whilst the red boxplots represent the errors from the maximum likelihood estimator.

the robust estimator of κ_ρ is accurate for high input values of κ_ρ (low noise), but can overestimate κ_ρ by up to 8% for small values of κ_ρ (higher noise). This trend is consistent across the three scenarios and ρ-values. In contrast, the performance of the maximum likelihood estimator is distinctly worse as the number of turns increases and ρ decreases. The unconditional concentration parameter κ_μ depends on both ρ and κ_ρ through the relationship $\kappa_\mu = (1-\rho^2)\kappa_\rho$.

Figure 5 shows the performance of the our algorithms, compared to the sliding window algorithm of Potts et al. (2018), as we vary the number of the turning points (m), the concentration parameter (κ), and the autocorrelation parameter (ρ), with the F1-score used as the evaluation metric. Several conclusions can be drawn from these results. First, both of our proposed models—angular AR(1) and IID—show very similar performance, particularly when the autocorrelation parameter ρ is small. For values of $\rho \leq 0.50$, both models achieve near-perfect F1-scores, indicating that their segmentation accuracy is excellent in scenarios with low autocorrelation.

Second, the F1-score decreases as ρ increases, reflecting the growing difficulty of the segmentation task as autocorrelation strengthens. However, this decline is not uniform across the different methods or scenarios. The angular AR(1) model exhibits a slower drop in performance compared to the IID model spatially for the extreme value.

Third, the concentration parameter κ_ρ appears to play a crucial role in how well the models handle increasing autocorrelation. For higher values of κ_ρ, both angular AR(1) and IID maintain their strong performance for a wider range of ρ, whilst the decline in F1-score becomes more pronounced at lower κ_ρ values. This suggests that the accuracy of these models in high-autocorrelation scenarios depends not only on ρ but also on κ_ρ, with smaller concentration parameters potentially amplifying the challenges posed by increasing autocorrelation. Overall, whilst both angular AR(1) and IID methods perform well in scenarios with low to moderate autocorrelation, the sliding window method is less accurate in such conditions, especially as ρ increases and m decreases. Figure 5 shows the F1-score using a

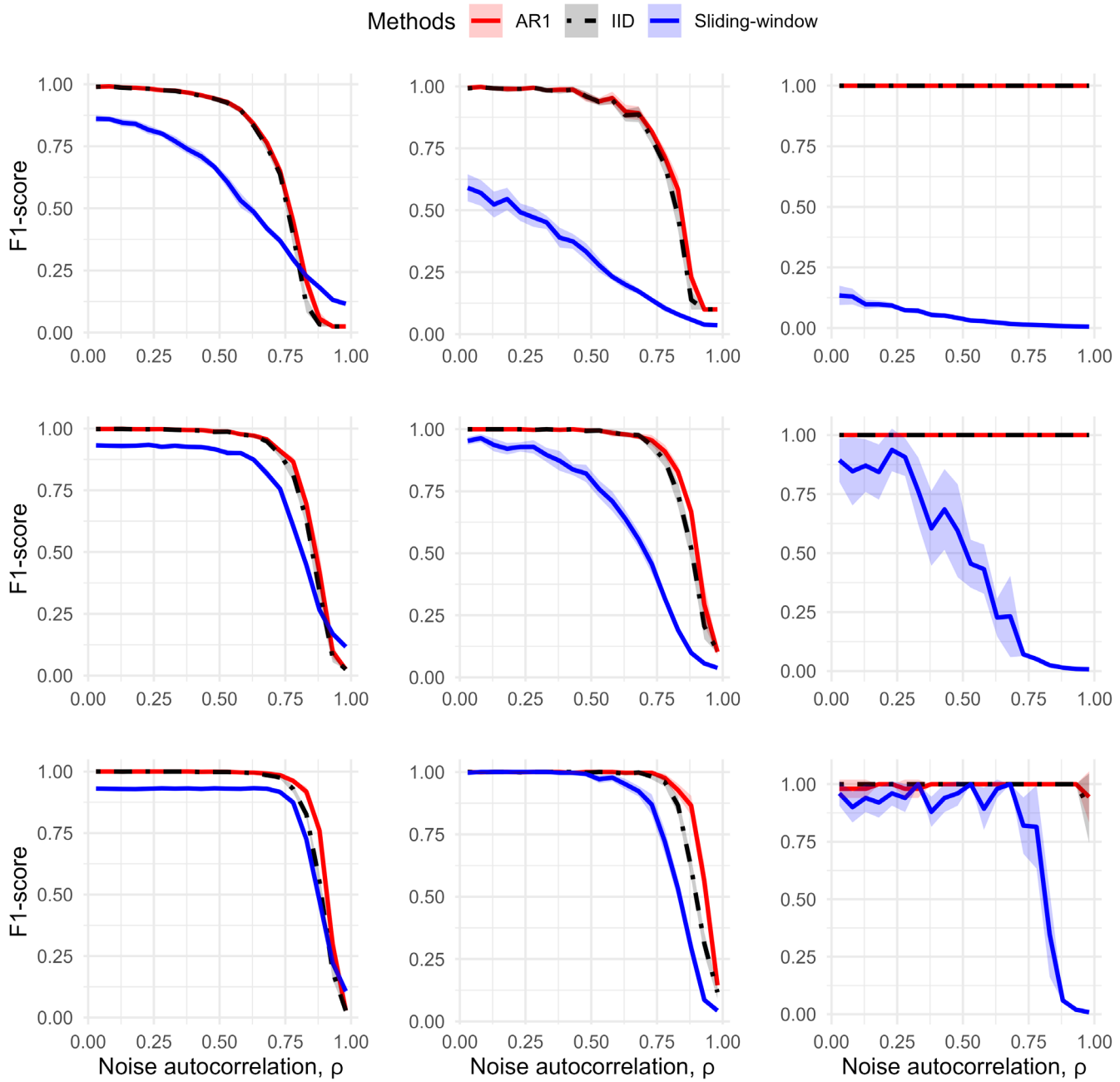

FIGURE 5 F1-score (Equation 21) as a function of the autocorrelation parameter ρ, comparing the performance of three methods: angular AR(1) (red), IID (black), and sliding window (blue). The first row presents the results for scenarios A, B and C (see Section 2.4), with $\kappa_\rho = 5, 15$ and 45 in each row, respectively.

window tolerance of 10 time points. Increasing the acceptance window slightly improves the F1-score, but the overall effect remains minimal. These results illustrate the methods' accuracy robustness to different acceptance criteria (see Appendix B in the Supporting Information).

3.2 | Oryx data

Figure 6 shows the result of using our algorithm to find turning points in an oryx path. The observed bearings suggest that the animal alternates between two main directions. The circular autocorrelation function of the residuals reveals a gradual, exponential-like decay in autocorrelation as the lag increases (Figure 7c). This pattern indicates strong autocorrelation starting at $\rho = 0.981$ at lag 1 and remaining significant over numerous lags before eventually approaching zero. Such behaviour is characteristic of an angular AR(1) process with a high autoregressive parameter. Additionally, the noise is highly concentrated, suggesting a large value of κ_ρ (Figure 6d).

Table 1 summarises the parameter estimates inferred for each of the six oryx paths using the IID and angular AR(1) models. The results of the two models do not exhibit consistent patterns. Both sets

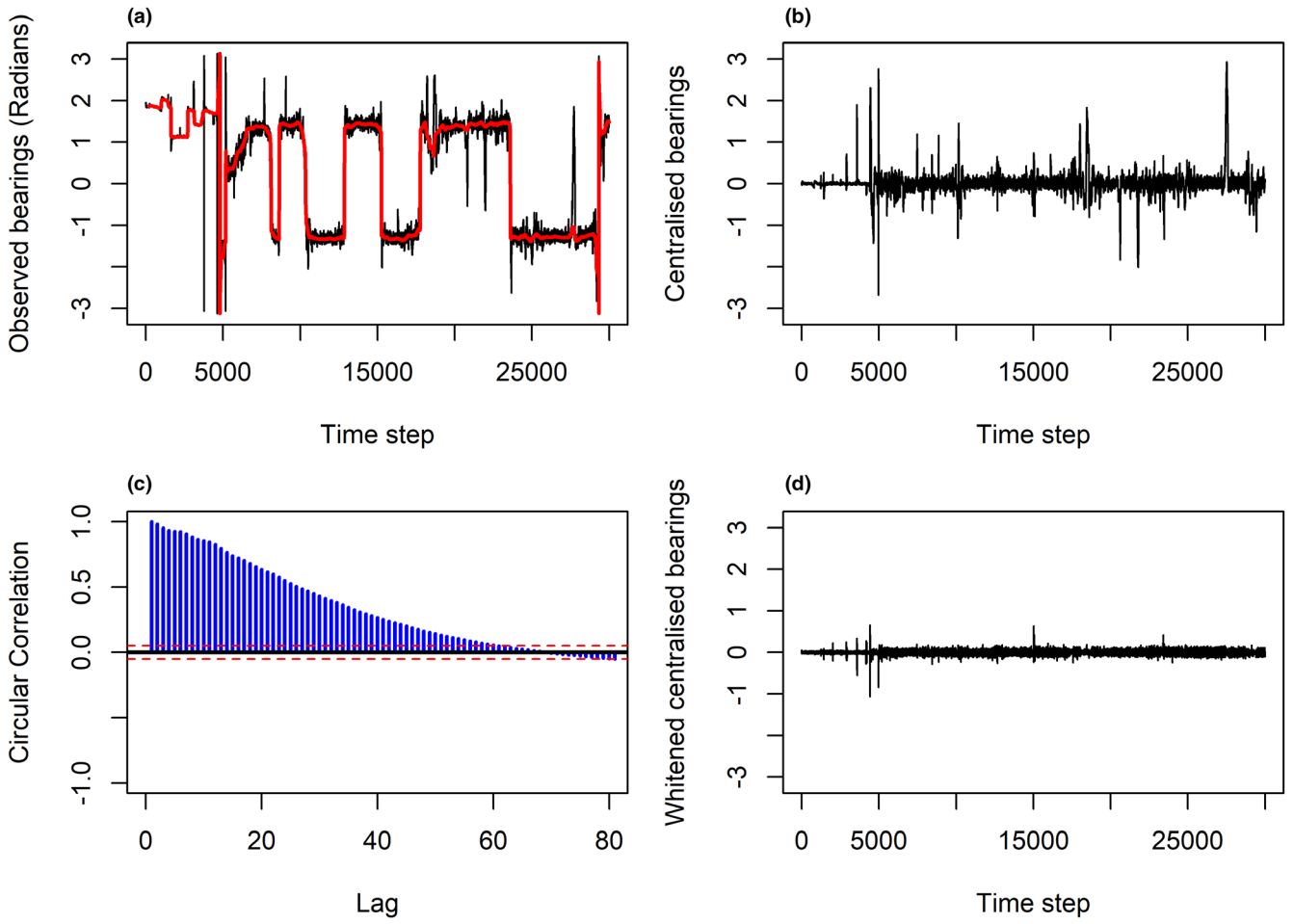

FIGURE 6 Inferring turning points from oryx data. (a) The observed bearing data (black) with the moving median estimate overlaid (red). (b) Centralised bearings based on the moving median. (c) Circular autocorrelation of the residuals. (d) Whitened centralised bearings after accounting for autocorrelation.

of estimates differ slightly from those reported by Potts et al. (2018; Table 1). Nevertheless, all three algorithms identify the most visually obvious turning points, although they vary in their sensitivity to whether small apparent turns are classified as true turning points (Figure 7).

Our implementation of the algorithms is coded in C++ and wrapped into R. The algorithms segmented a profile of length $n = 10^6$ in 3 and 7 s for the IID and angular AR(1) models, respectively, on a desktop computer equipped with an Intel Core i7-6700U CPU (2.40 GHz, four cores) and 32 GB of RAM. The discretisation level was set to $\frac{\pi}{360}$ in the angular AR(1) case. These runtimes scaled linearly with n.

4 | DISCUSSION

We have described two fast, accurate model-based algorithms that provide a description of an animal's movement in terms of straight-line segments interspersed with turns. Our approach consists of two main stages. In the first stage, we construct estimators for the extent of autocorrelation in the noise, given by ρ, and the magnitude of the noise, given by $1/\kappa$, where κ is the concentration parameter of a von Mises distribution of error. We detail two methods for this purpose. The first method involves estimating κ and ρ using the angular successive differences of the observations at the first lag. The second method applies a simple moving median filter to estimate the mean steps, followed by estimating κ and ρ based on the residuals (Section 2.3).

An alternative approach might involve making an initial guess of ρ and κ, estimating the turning points, iteratively refining the parameters based on the fitted model, and then updating parameters until the results stabilise. However, our experiments (not detailed here) show that this method can be sensitive to the initial guess, potentially leading to an incorrect number of turning points. Furthermore, model misspecification of the underlying process can reduce the accuracy of the parameter estimates.

In the second stage, we use the estimated values of κ and ρ to identify turning points by maximising a particular penalised likelihood. For this we use a version of the FPOP algorithm, modified for use with circular statistics. An alternative approach for accurately determining the optimal solution for identifying turning points, without approximating the space of possible headings, μ,

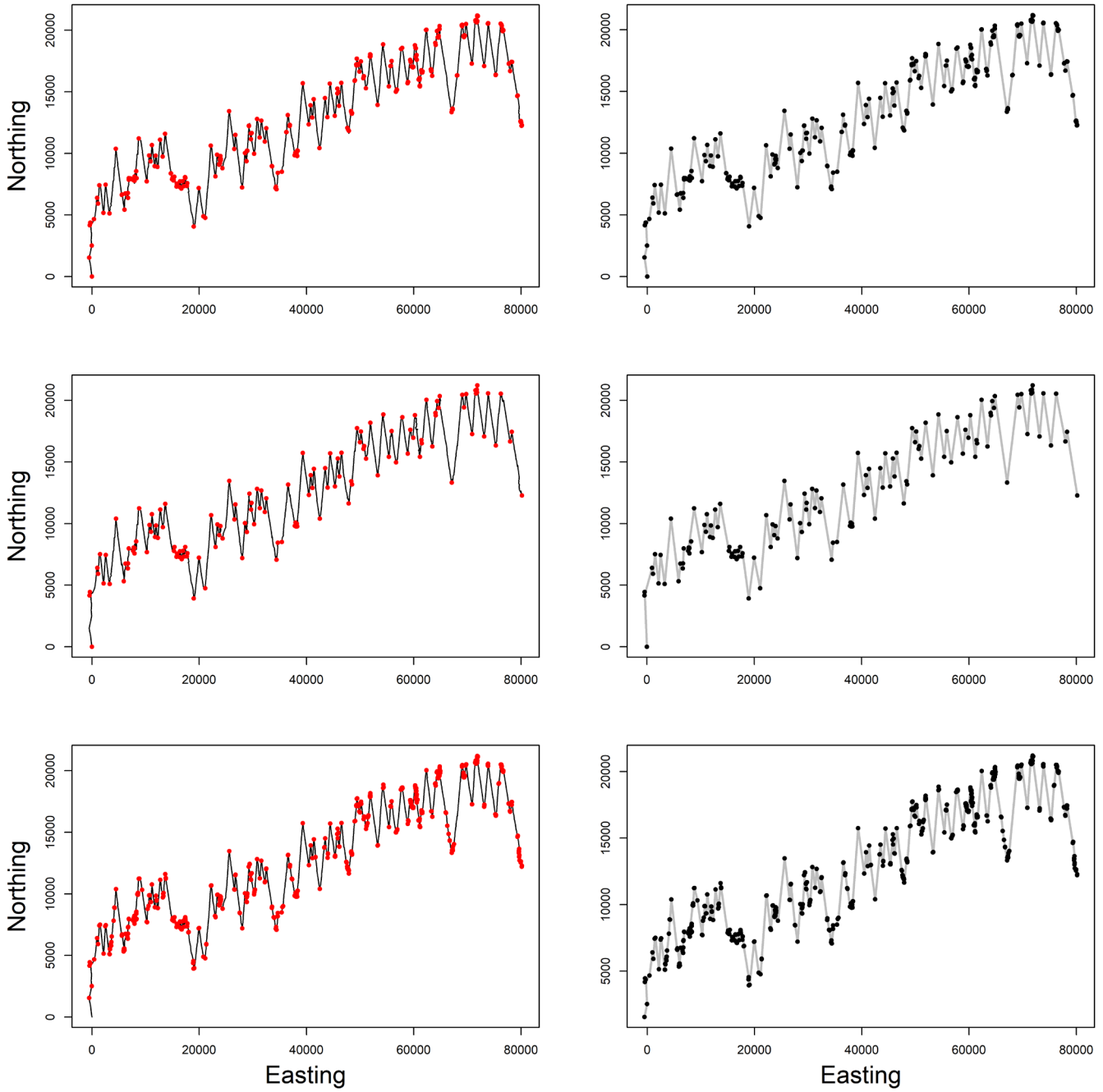

FIGURE 7 An oryx path reconstructed from magnetometer data, assuming constant speed. The first column displays the path of a single oryx, where the red dots in the top row show the inferred turning points using the angular AR(1) model. In the second row, turning points are inferred using the IID model, and in the third row they are inferred using the sliding window algorithm. The second column shows the resulting models of the path as a series of steps and turns.

TABLE 1 The results of estimating the turning points in the oryx data.

ID	κ_ρ	κ_μ	ρ	m(AR(1))	m(IID)	σ(AR(1))	σ(IID)
1	353.052	7.257	0.981	315	137	0.061	0.041
2	226.496	5.098	0.985	113	127	0.079	0.067
3	44.790	3.215	0.957	102	97	0.206	0.083
4	228.314	4.078	0.990	24	32	0.092	0.084
5	90.784	3.255	0.976	52	71	0.107	0.115
6	53.940	2.607	0.974	47	76	0.156	0.106

under the angular AR model, involves employing the pruned exact linear time (PELT) method (Killick et al., 2012). Although PELT may not outperform our approach in speed, under certain conditions it does offer a linear time complexity for the segmentation process, making it a competitive option. As our fitting of the angular AR(1) model is based on the discretisation of the space of possible headings μ, we recommend setting the discretisation level to $\frac{\pi}{360}$ radians, as a result of a simulation experiment (not detailed here) in which it was observed that adding more resolution does not improve segmentation. For the IID model, robustness can be further enhanced by substituting the cosine component with a wrapped version of the biweight loss function, as described by Fearnhead and Rigaill (2019).

We evaluated our methods using both real and simulated data. Given a path consisting of straight moves and turns, where headings are measured with a standard deviation accuracy of $\frac{\pi}{12}$ radians and the noise autocorrelation is less than 0.5, our algorithms successfully identify nearly 100% of the turning points. This level of accuracy compares favourably with previous widely used method described by Potts et al. (2018), which our method significantly improves upon (Figure 5).

Detecting turning points is a particular case of detecting change-points (also known as break-points), which involves detecting abrupt changes in the statistical properties of a time series, such as mean, variance, trend, regression coefficients, and autoregressive coefficients. Change-point detection is currently an active research area in statistics and machine learning due to its relevance across various applications. This includes not only animal movement studies but also a diverse range of fields such as calcium imaging data analysis (Jewell et al., 2020; Jewell & Witten, 2018), analysis of DNA sequences (Muggeo & Adelfio, 2011), and environmental data analysis (Kehagias, 2002). Although our methods are primarily motivated by ecological applications, they have potential for detecting change-points in angular data in other contexts (e.g. change in wind direction or wave direction).

We have outlined different approaches for segmenting high-frequency movement data, each suited to specific analytical needs. First, when estimating the autocorrelation parameter, the simplest method involves using estimates based on successive movements. However, extreme autocorrelation values (very close to one) can lead to invalid measures, occasionally exceeding one. In such cases, it becomes necessary to either impose an upper limit or adopt a non-parametric approach to ensure valid estimates.

Estimating ρ using the robust method shows a small but consistent bias in some simulation scenarios, particularly when the noise concentration κ_ρ is low, with the worst-case bias not exceeding 0.15. This suggests that in situations with high noise and moderate autocorrelation, the method may slightly overestimate the true level of autocorrelation. However, this bias becomes negligible as κ_ρ increases, with estimates becoming nearly unbiased for $\kappa_\rho \geq 45$ and $\rho = 0.98$. Whilst the bias is relatively small, it is important to acknowledge it as a potential source of imprecision in downstream inference. In particular, such biases could cumulatively affect the estimation of the concentration parameters, and in turn, influence the accuracy of the turning points inference.

Our framework highlights linear movement segments punctuated by discrete turning points. This assumption generally holds well across many datasets (Gunner et al., 2024). However, there are cases where external factors such as terrain, wind or water currents cause animals to follow curved paths instead of straight ones. In such cases, it becomes important to consider and, where possible, correct for these external influences before identifying true behavioural turns.

Still, the goal of our framework is to capture the structure of movement across a wide range of behaviours. Sometimes, these are characterised by relatively high-frequency turns at small spatial scales, for example the tracks of grazing herbivores. Other times, turns may be much less frequent, interspersed with long sections of straight movement, for example when moving towards a distant goal. There may also be situations that involve turning at multiple spatial scales, for example when moving to a distant goal through a landscape containing obstacles to movement (trees, rocks, fences etc.). All such behaviours, though, involve detection of turning points as a primary stage, before we can ask the question as to why these turns were made.

Indeed, turning points represent decisions made by the animal, which can play an important role in further analyses, such as step selection analysis and state-space models. Such approaches tend to view animal trajectories as a series of step lengths and turning angles, calculated at regular intervals, often at low frequency (Patterson et al., 2017). However, replacing these with more behaviourally driven step-turn metrics might improve inference, as it better reflects the animal's decisions compared to calculations based on regularly subsampled locations. Indeed, this has already been shown for step selection analysis (Munden et al., 2021). Ongoing work by some of the present authors investigates whether this is true for other tools in animal movement analysis, such as hidden Markov models (Langrock et al., 2012; Michelot et al., 2016).

Our method is designed for data collected using high-frequency magnetometers or modern GPS devices capable of sampling at 1 Hz over extended periods (Nathan et al., 2022). By high-frequency, we mean that there are enough data points between successive turns to be able to identify them robustly. Whilst we did not perform a detailed analysis to find the lower limit of number of datapoints between turns, our simulated data included turns interspersed by as little as 17 datapoints. Our procedure for assessing accuracy of inference relies on a tolerance of ± 10 datapoints, so to be consistent with this, we suggest that data ought to be sufficiently high frequency that there is highly unlikely to be <10 measured locations between successive turns. For lower frequency data, on a timescale closer to that of the turns, it is necessary to use an approach that is explicitly formulated in continuous time. Blackwell (2025) describes such a method, which reconstructs the precise times of

turns between observations, but it is not computationally competitive with the methods introduced here.

Lastly, whilst our method examines the data as a stream of headings at each time step, we implicitly assume that the animal is moving between each observation, which may not always hold in practice. If that is a concern and velocity information is available (e.g. from accelerometer or locational data), incorporating such data into the analysis or post-processing our inferences could ensure that the detected turns align with times when this assumption is satisfied (Gunner et al., 2024).

AUTHOR CONTRIBUTIONS

Jonathan R. Potts and Paul G. Blackwell conceived the idea. Abdulmajeed F. Alharbi designed the methodology, performed the research and led the writing of the manuscript. Abdulaziz Alagaili, Nigel C. Bennett and David Michael Scantlebury provided data. All authors contributed critically to the drafts and gave final approval for publication.

ACKNOWLEDGEMENTS

This work was partly funded by King Saud University in Saudi Arabia through their employee sponsorship programme for doctoral research projects. Fieldwork and data collection for the oryx data were funded by the ongoing Research Funding program, Research Chairs (ORF-RC-2025-1900), King Saud University, Riyadh, Saudi Arabia. We are also grateful to Prince Bander bin Saud Al-Saud, former President of the Saudi Wildlife Authority (SWA), for his support in undertaking these studies.

CONFLICT OF INTEREST STATEMENT

The authors have no conflicts of interest to declare.

PEER REVIEW

The peer review history for this article is available at https://www.webofscience.com/api/gateway/wos/peer-review/10.1111/2041-210x.70221.

DATA AVAILABILITY STATEMENT

Code available via https://zenodo.org/records/17634203 (Alharbi, 2025). Oryx data available via https://orda.shef.ac.uk/articles/dataset/Oryx_headings/6605330 (Potts et al., 2018).

ORCID

Abdulmajeed F. Alharbi https://orcid.org/0009-0009-5522-1496
Paul G. Blackwell https://orcid.org/0000-0002-3141-4914
David Michael Scantlebury https://orcid.org/0000-0001-8327-0556
Jonathan R. Potts https://orcid.org/0000-0002-8564-2904

REFERENCES

Alharbi, A. (2025). F3bdulmajeed/turning-points-detection: Identification of turning points in high-frequency animal movement data (release). *Zenodo*. https://doi.org/10.5281/zenodo.17634203

Avgar, T., Potts, J. R., Lewis, M. A., & Boyce, M. S. (2016). Integrated step selection analysis: Bridging the gap between resource selection and animal movement. *Methods in Ecology and Evolution*, *7*(5), 619–630.

Bardwell, L., Fearnhead, P., Eckley, I. A., Smith, S., & Spott, M. (2019). Most recent changepoint detection in panel data. *Technometrics*, *61*(1), 88–98.

Bidder, O., Walker, J., Jones, M., Holton, M., Urge, P., Scantlebury, D., Marks, N., Magowan, E., Maguire, I., & Wilson, R. (2015). Step by step: Reconstruction of terrestrial animal movement paths by dead-reckoning. *Movement Ecology*, *3*(1), 1–16.

Blackwell, P. G. (2025). *Bayesian inference for velocity-jump models for movement*. arXiv Preprint, 2509.21226.

Boulinier, T., Kada, S., Ponchon, A., Dupraz, M., Dietrich, M., Gamble, A., Bourret, V., Duriez, O., Bazire, R., Tornos, J., Tveraa, T., Chambert, T., Garnier, R., & McCoy, K. D. (2016). Migration, prospecting, dispersal? What host movement matters for infectious agent circulation? *Integrative and Comparative Biology*, *56*(2), 330–342.

Chakar, S., Lebarbier, E., Lévy-Leduc, C., & Robin, S. (2017). A robust approach for estimating change-points in the mean of an AR(1) process. *Bernoulli*, *23*(2), 1408–1447. https://doi.org/10.3150/15-BEJ781

Cleynen, A., Koskas, M., Lebarbier, E., Rigaill, G., & Robin, S. (2014). Segmentor3isback: An r package for the fast and exact segmentation of seq-data. *Algorithms for Molecular Biology*, *9*, 1–11.

Codling, E. A., & Plank, M. J. (2011). Turn designation, sampling rate and the misidentification of power laws in movement path data using maximum likelihood estimates. *Theoretical Ecology*, *4*, 397–406.

Fearnhead, P., & Rigaill, G. (2019). Changepoint detection in the presence of outliers. *Journal of the American Statistical Association*, *114*(525), 169–183.

Fryzlewicz, P. (2014). Wild binary segmentation for multiple change-point detection. *The Annals of Statistics*, *42*(6), 2243–2281.

Grainger, D., & Blackwell, P. G. (2025). Finch: Fast statistical inference for continuous-time animal movement. *Methods in Ecology and Evolution*, *16*, 1437–1459.

Gunner, R., Wilson, R., Lurgi, M., Borger, L., Redcliffe, J., Shepard, E., Holton, M., Crofoot, M., Alagaili, A., Andrzejaczek, S., Ariano-Sánchez, D., Barbedette-Gerard, T., Bennett, N., Bernard, A., Brown, R., Cole, N., Creel, S., Cruz-Neto, A., di Virgilio, A., … Potts, J. (2024). High resolution data reveal fundamental steps and turning points in animal movements. *Research Square*, 1–29. https://doi.org/10.21203/rs.3.rs-5559169/v1

Jammalamadaka, S. R., & Sarma, Y. R. (1988). A correlation coefficient for angular variables. In *Statistical theory and data analysis II* (pp. 349–364). North Holland.

Jewell, S., & Witten, D. (2018). Exact spike train inference via l0 optimization. *The Annals of Applied Statistics*, *12*(4), 2457.

Jewell, S. W., Hocking, T. D., Fearnhead, P., & Witten, D. M. (2020). Fast nonconvex deconvolution of calcium imaging data. *Biostatistics*, *21*(4), 709–726.

Katzner, T., & Arlettaz, R. (2020). Evaluating contributions of recent tracking-based animal movement ecology to conservation management. *Frontiers in Ecology and Evolution*, *24*, 519.

Kehagias, A. (2002). *Hidden Markov model segmentation of hydrological and enviromental time series*. arXiv preprint, cs/0206039.

Killick, R., Fearnhead, P., & Eckley, I. A. (2012). Optimal detection of changepoints with a linear computational cost. *Journal of the American Statistical Association*, *107*(500), 1590–1598.

Klappstein, N. J., Thomas, L., & Michelot, T. (2023). Flexible hidden Markov models for behaviour-dependent habitat selection. *Movement Ecology*, *11*(1), 30.

Langrock, R., King, R., Matthiopoulos, J., Thomas, L., Fortin, D., & Morales, J. M. (2012). Flexible and practical modeling of animal telemetry data: Hidden Markov models and extensions. *Ecology*, *93*(11), 2336–2342.

Lavielle, M., & Moulines, E. (2000). Least-squares estimation of an unknown number of shifts in a time series. *Journal of Time Series Analysis*, *21*(1), 33–59.

Lewis, K. P., Vander Wal, E., & Fifield, D. A. (2018). Wildlife biology, big data, and reproducible research. *Wildlife Society Bulletin*, *42*(1), 172–179.

Maidstone, R., Hocking, T., Rigaill, G., & Fearnhead, P. (2017). On optimal multiple changepoint algorithms for large data. *Statistics and Computing*, *27*, 519–533.

Michelot, T., Langrock, R., & Patterson, T. A. (2016). Movehmm: An r package for the statistical modelling of animal movement data using hidden Markov models. *Methods in Ecology and Evolution*, *7*(11), 1308–1315.

Muggeo, V. M., & Adelfio, G. (2011). Efficient change point detection for genomic sequences of continuous measurements. *Bioinformatics*, *27*(2), 161–166.

Munden, R., Börger, L., Wilson, R. P., Redcliffe, J., Brown, R., Garel, M., & Potts, J. R. (2021). Why did the animal turn? Time-varying step selection analysis for inference between observed turning-points in high frequency data. *Methods in Ecology and Evolution*, *12*(5), 921–932.

Nathan, R., Getz, W. M., Revilla, E., Holyoak, M., Kadmon, R., Saltz, D., & Smouse, P. E. (2008). A movement ecology paradigm for unifying organismal movement research. *Proceedings of the National Academy of Sciences*, *105*(49), 19052–19059.

Nathan, R., Monk, C. T., Arlinghaus, R., Adam, T., Alós, J., Assaf, M., Baktoft, H., Beardsworth, C. E., Bertram, M. G., Bijleveld, A. I., Brodin, T., Brooks, J. L., Campos-Candela, A., Cooke, S. J., Gjelland, K. Ø., Gupte, P. R., Harel, R., Hellström, G., Jeltsch, F., … Jarić, I. (2022). Big-data approaches lead to an increased understanding of the ecology of animal movement. *Science*, *375*(6582), eabg1780.

Patterson, T. A., Parton, A., Langrock, R., Blackwell, P. G., Thomas, L., & King, R. (2017). Statistical modelling of individual animal movement: An overview of key methods and a discussion of practical challenges. *AStA Advances in Statistical Analysis*, *101*, 399–438.

Potts, J. R., Börger, L., Scantlebury, D. M., Bennett, N. C., Alagaili, A., & Wilson, R. P. (2018). Finding turning-points in ultra-high-resolution animal movement data. *Methods in Ecology and Evolution*, *9*(10), 2091–2101.

Turchin, P., Odendaal, F., & Rausher, M. (1991). Quantifying insect movement in the field. *Environmental Entomology*, *20*(4), 955–963.

Williams, H. J., Taylor, L. A., Benhamou, S., Bijleveld, A. I., Clay, T. A., de Grissac, S., Demšar, U., English, H. M., Franconi, N., Gómez-Laich, A., Griffiths, R. C., Kay, W. P., Morales, J. M., Potts, J. R., Rogerson, K. F., Rutz, C., Spelt, A., Trevail, A. M., Wilson, R. P., & Börger, L. (2020). Optimizing the use of biologgers for movement ecology research. *Journal of Animal Ecology*, *89*(1), 186–206.

SUPPORTING INFORMATION

Additional supporting information can be found online in the Supporting Information section at the end of this article.

Figure A.1. A simple example showing the function $F(t, \mu)$ for the first two iterations.

Figure A.2. Line plots of the F1-score under noise with non-constant κ, as a function of the autocorrelation parameter ρ, comparing the performance of three methods: angular AR(1) (red), IID (black) and sliding-window (blue).

Figure A.3. Line plots of the F1-score with wrapped normal noise as a function of the autocorrelation parameter ρ, comparing the performance of three methods: angular AR(1) (red), IID (black) and sliding-window (blue).

Figure A.4. Line plots of the F1-score with angular AR(3) noise as a function of the autocorrelation parameter ρ, comparing the performance of three methods: angular AR(1) (red), IID (black) and sliding-window (blue).

Figure A.5. Line plots of the F1-score with MA(10) noise as a function of the autocorrelation parameter ρ, comparing the performance of three methods: AR(1) (red), IID (black) and sliding-window (blue).

Figure A.6. Sensitivity analysis of F1-score under varying acceptance rules for scenario A.

Figure A.7. Sensitivity analysis of F1-score under varying acceptance rules for scenario B.

Figure A.8. Sensitivity analysis of F1-score under varying acceptance rules for scenario C.

Figure A.9. Error in estimation of ρ under the different scenarios from Section 2.4.

How to cite this article: Alharbi, A. F., Blackwell, P. G., Alagaili, A., Bennett, N. C., Scantlebury, D. M., & Potts, J. R. (2025). Efficient statistical inference of turning points in animal movement data. *Methods in Ecology and Evolution*, *00*, 1–14. https://doi.org/10.1111/2041-210x.70221